Research Square

Preprints are preliminary reports that have not undergone peer review.
They should not be considered conclusive, used to inform clinical practice,
or referenced by the media as validated information.

On Channel Estimation for Rician fading with the phase-shift in Cell-Free Massive MIMO system

Jamal Amadid (jamal.amadid@edu.uca.ac.ma)
Universite Cadi Ayyad Faculte des Sciences Semlalia https://orcid.org/0000-0002-6158-069X
Mohamed boulouird
Cadi Ayyad University: Universite Cadi Ayyad
Abdelfettah Belhabib
Universite Cadi Ayyad Faculte des Sciences Semlalia
Abdelouhab Zeroual
Universite Cadi Ayyad Faculte des Sciences Semlalia

Research Article

Keywords: Channel Estimation, Massive MIMO, Cell-Free, Rician Fading, Phase-Shift

Posted Date: April 13th, 2021

DOI: https://doi.org/10.21203/rs.3.rs-351172/v1

License: This work is licensed under a Creative Commons Attribution 4.0 International License.
Read Full License

Version of Record: A version of this preprint was published at Wireless Personal Communications on December 2nd, 2021. See the published version at https://doi.org/10.1007/s11277-021-09436-6.

Noname manuscript No.
(will be inserted by the editor)

On Channel Estimation for Rician fading with the phase-shift in Cell-Free Massive MIMO system

Jamal Amadid[1] · **Mohamed Boulouird**[2] · **Abdelfettah Belhabib**[1] · **Abdelouhab Zeroual**[1]

Received: date / Accepted: date

Abstract Channel estimation (CE) is a crucial phase in wireless communication systems, especially in cell-free (CF) massive multiple input multiple output (M-MIMO) since it is a dynamic wireless network. Therefore, this work is introduced to study CE for CF M-MIMO system in the uplink phase, wherein the performance of different estimators are evaluated, discussed, and compared in various situations. We assume the scenario in which each access point has prior knowledge of the channel statistics. The phase-aware-minimum mean square error (PA-MMSE) estimator, the non-phase-aware-MMSE (NPA-MMSE) estimator, and the least-squares estimator are the three estimators which are exploited in this work. Besides, we consider the Rician fading channel in which the line-of-sight path is realized with a phase-shift that models the users' mobility where the considered phase-shift follows a uniform distribution. On the other hand, the mean-squared error metric is employed in order to evaluate the performance of each estimator, where an analytical and simulated result is provided for the PA-MMSE estimator and the NPA-MMSE estimator in order to assert our numerical results.

Keywords Channel Estimation · Massive MIMO · Cell-Free · Rician Fading · Phase-Shift

Jamal Amadid
E-mail: jamal.amadid@edu.uca.ac.ma

Mohamed Boulouird

Abdelfettah Belhabib
E-mail: abdelfettah.belhabib@edu.uca.ac.ma

Abdelouhab Zeroual

[1]Instrumentation, Signals and Physical Systems (I2SP) Group, Faculty of Sciences Semlalia, Cadi Ayyad University, Marrakesh, Morocco.

[2]Smart Systems and Applications (SSA) Group, National School of Applied Sciences of Marrakesh (ENSA-M), Cadi Ayyad University, Marrakesh, Morocco.

Declarations

Funding : Not applicable

Conflicts of interest/Competing interests : Not applicable

Availability of data and material : Not applicable

Code availability : Not applicable

Authors' contributions : Not applicable

Acronyms

5G : fifth generation
AP : access point
CB : coherence block
CF : cell-free
CE : channel estimation
CSI : channel state information
DL : downlink
EE : energy efficiency
MMSE : minimum mean square error
LS : least-squares
LoS : line-of-sight
LSF : large-scale fading
M-MIMO : massive multiple input multiple output
MSE : mean-squared error
NPA-MMSE : non-phase-aware-minimum mean square error
PA-MMSE : phase-aware minimum mean square error
PC : pilot contamination
PS : pilot sequence
SE : spectral efficiency
SSF : small-scale fading
UL : uplink

1 Introduction

The employment of a large number of antennas at the base stations knows, in the literature of communication systems as the massive multiple input multiple output (M-MIMO) technology [1], where this technology can offer good service to many users even if in the worst scenario, in which the users are simultaneously served [2,3]. Two types of antenna arrays are used in the M-MIMO wireless network literature, where

the antenna arrays can be either co-located or distributed. The co-located antenna scenarios have been defined in the literature as being located in a compacted array and have low backhaul demands [4]. On the other hand, with the distributed configuration of M-MIMO systems, the antennas are distributed over a wide geographical area [5–7]. This latter configuration known in the literature as cell-free (CF) M-MIMO. CF M-MIMO offers a significant gain for the fifth generation (5G) wireless communication systems, in which an enormous number of access points (APs) serve a relatively small number of users in the same time-frequency resources. The CF rely on the front-haul connection between APs [6] and using channels-based MIMO schemes to get a local channel state information (CSI) [8].
CF M-MIMO is an innovative technology that enables such a system to operate with a more important potential for 5G wireless communication using only a straightforward signal processing technique. In addition, this technology can offer energy efficiency (EE), substantial throughput, and high precision. In its basic canonical design, CF M-MIMO technology uses a large number of APs, assumed to be randomly located in a large area and serving a reasonably small number of users which are also assumed to be randomly distributed [9–11]. Thus, in many scenarios, some APs receive higher levels of interference compared to other APs depending on the user's location.
In CF M-MIMO, the whole network APs are engaged, coherently, to serve all users. The CF M-MIMO has a high potential to spatially multiplexing users and regulates the interference depending on the network design and architecture [5]. The distributed M-MIMO configuration (i.e., CF) affords an enhanced macro-diversity that contributes to a better EE and coverage probability contrary to the located M-MIMO configuration. Thereby, due to the increased demand for connectivity, and the requirement to provide users with good service, the distributed M-MIMO design is expected to provide much improvement for wireless communication systems. As a consequence, CF M-MIMO has garnered significant attention from researchers.

2 Related Works

The purpose of this section is to present the related works that have been addressed the CF M-MIMO. Besides, some work denominated this system as a distributed antennas system [12–15].
In [16], the authors investigate the spectral efficiency (SE) for a CF M-MIMO system that operates in both uplink (UL) and downlink (DL) using a Rician fading channel. A deterministic component is introduced to reflect the line-of-sight (LoS) propagation environment. Besides, a phase is joined with the deterministic component to draw the users' mobility. For the UL phase, a decoding scheme based on two-layers method is introduced to overcome the interference, namely, coherent and incoherent interference. On the other hand, in the DL stage, two distinct transmission manners are investigated in which they are named these transmissions as incoherent and coherent transmission.
In [17], the authors propose a beamforming-based technique for CF M-MIMO systems that operates under time division duplex protocol which obeys the constraint defined by short-term average power for this network type (i.e., CF network). Fur-

thermore, the impact of imperfect channel knowledge is considered. Analytical and numerical results are presented to compare the proposed beamforming scheme and the traditional beamforming. The authors concluded that an improved result is obtained in terms of the achievable rate using the proposed beamforming strategy.
In [18], the authors deal with network MIMO, where a large number APs serve a relatively small number of users, which recently called CF M-MIMO, where it provides a much improvement for wireless communication systems. The authors have introduced an innovative idea, namely, the scalability of a CF network. CF M-MIMO is said to be scalable, even though in a situation with an infinite number of serving users, we can guarantee that the complexity can be finite. This concept is investigated using a dynamic cooperation cluster that has been treated previously for network MIMO. Besides, The pilot assignment and the formation of clusters are studied under the scalability concept and in the same way for channel estimation (CE), combining, and precoding schemes. Moreover, a distributed and centralized processes are studied, whereas the authors concluded that both modes provide the same CE quality since the backhaul is considered without loss.
The authors in [19] have addressed the hardware weakness, and their influence over CF M-MIMO since the antenna quality confronts guaranteeing good communication between transceivers. The SE and EE are investigated for both links (i.e., UL and DL), whereas in each situation, a closed-form expression is driven for each stage. However, under the goal of maximizing the user rate. The power control algorithm, i.e. max-min, is adopted. Finally, the authors provide analytical and numerical results for the sake of affirming the theoretical study.
An UL stage for CF M-MIMO has been investigated in [20], where the authors have considered the most realistic scenario in which the channels are correlated. Besides, considering the Rician fading channel. On the other hand, SE is studied using various estimators. The authors presented Results to assert theoretical expressions. Conclude that the correlation among channels is beneficial for SE. Additionally, deteriorating performance is obtained using a linear MMSE estimator, which is explained by the fact that it has no phase knowledge.
After presenting the previous works to the best of our knowledge on the CF M-MIMO. The work organization is presented below

2.1 Organization

The rest of this work is structured in the following form : The CF system model is presented in **Section 3**, where the Rician fading channel is introduced. **Section 4** investigates UL CE using various channel estimators (i.e., (least-squares) LS, phase-aware-minimum mean square error (PA-MMSE), non-phase-aware-minimum mean square error (NPA-MMSE)), where the mean-squared error (MSE) expression for each estimator is given. The numerical results are presented in **Section 5**, with which we assert our analytical expressions given in the previous sections. **Section 6** presents the conclusion and future work.

2.2 Conributions of this work

The principal contributions of this work are outlined as follows

1. Studying CE using the Rician fading channel in which the LoS path is used in each communication link (i.e., each communication that links a particular user to a particular AP).
2. Investigate and evaluate the influence of previous knowledge of the phase-shift over the CE using the PA-MMSE estimator. In addition, evaluate CE quality without any previous knowledge using the NPA-MMSE estimator.

3 Cell-Free System Model

In this section, we present the system model used, as shown in Fig. (1) below, where all users and all APs are considered outfitted with a single antenna. It is important to note that the multi-antenna AP situation can be constructed using a single antenna AP by handling each antenna of a multi-antenna AP as an independent AP. We studied and evaluated the uncorrelated channel model in which the small-scale fading (SSF) coefficients are not correlated, as indicated in [21]. On the other hand, we assume that the channel is flat fading over each coherence block (CB) that comports τ_c frequency (i.e., τ_c indicates the CB length). The CB length is affected by many factors, such as the users' velocity, number of wavelengths, and spreading environment [22]. The channel coefficient that links the k_{th} user to the m_{th} AP is formulated as follows

$$g_{m,k} = \bar{g}_{m,k} e^{j\chi_{m,k}} + \Theta_{m,k} \tag{1}$$

Here, $\Theta_{m,k}$ symbolizes the channel gain that corresponds to the Non-LoS path between the k_{th} user and the m_{th} AP. In addition, this channel gain can be formulated as $\Theta_{m,k} \sim \mathscr{N}_{\mathscr{C}}(0, \beta_{m,k})$, where $\beta_{m,k}$ signifies the large-scale fading (LSF) coefficient that encompassing the shadow fading and path-loss. On the other hand, the gain $\bar{g}_{m,k}$ is a positive coefficient (i.e., $\bar{g}_{m,k} \geq 0$) that denotes the LoS path components, and $\chi_{m,k} \sim \mathscr{U}[-\pi, \pi]$ symbolizes de phase-shift. It is important to highlight that the channel gain indicated in equation (1) follows the Rician distribution and is called the Rician fading model because $|g_{m,k}|$ is Rice distributed. Furthermore, $g_{m,k}$ does not follow a Gaussian distribution as in numerous studies that overlook the phase-shift. Assuming that the channel is considered an independent random variable for each user-AP link and the channel realizations over various CBs are independent and identically distributed.

4 Uplink Channel Estimation

The CB is the time-frequency interval over which the channel that connects a user to his serving AP is considered unchanged. This interval length is τ_c, which defines the number of frequencies used in each CB. Each CB is assumed to be divided into portions. One of this portion is the UL Pilot Sequence (PS) which has the length τ_p and must be obey the following constraints $\tau_c > \tau_p$. In the slot τ_p, all users dispatch

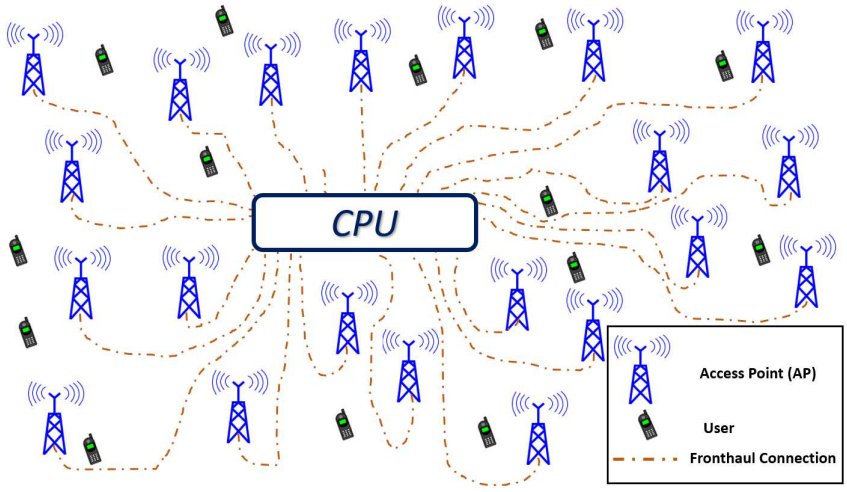


Fig. 1 Typical representation of a CF M-MIMO grid

their PSs for the sake of communicating with its serving APs (where a very small interval comes after dispatching the pilot, namely, the CE process as mentioned in [23]). Thereby, because of the limited CB length, which also depends on the many environmental factors. In addition, we use the frequency reuse technique in order to obey this constraint where this frequency reuse leads to a known phenomenon in the literature of wireless communication systems, namely, Pilot Contamination (PC).
The UL pilot length is τ_p, i.e., the system can benefit from the τ_p orthogonal pilot (τ_p users can use orthogonal pilots where the remaining users reuse the same pilots, which are already assigned to the first τ_p users). We consider that the k_{th} user dispatched the PS $\psi_k \in \mathbb{C}^{\tau_p \times 1}$ that meets the following requirements $\|\psi_k\|^2 = \tau_p$. The obtained signal $\mathbf{y}_m^p$ at the m_{th} AP is expressed as

$$\mathbf{y}_m^p = \sum_{k=1}^{K} \sqrt{q_k} g_{m,k} \psi_k + w_m^p \tag{2}$$

Here, $\mathbf{y}_m^p \in \mathbb{C}^{\tau \times 1}$ indicates the spread vector and $w_m^p \sim \mathcal{N}_C(0_{\tau_p}, \sigma^2 \mathbb{1}_{\tau_p})$ denotes the noise. In order to estimate the channel $g_{m,k}$, an adequate statistic is used, where the m_{th} AP calculate the inner product of the obtained signal and the dispatched PS from the k_{th} user. This statistic increases the degree of freedom and provides a signal without depending on the PS. The expression of the obtained signal is written as

$$y_{m,k}^p = \psi_k^H \mathbf{y}_m^p = \sum_{j=1}^{K} \sqrt{q_j} g_{m,j} \psi_k^H \psi_j + \psi_k^H w_m^p \tag{3}$$

In CF M-MIMO, generally speaking, the number of users is large relative to the PS length (i.e., $K > \tau_p$). Thus, we consider a set $\mathcal{P}_k$ of users employing the same pilot as the k_{th} user, counting itself as well. It is important to note that users with a different

PS (i.e., orthogonal PS) have their product equal to zero (i.e., $\psi_k \psi_i = 0, \forall k \neq i$).

$$y^p_{m,k} = \sqrt{q_k}\tau_p g_{m,k} + \sum_{j \in \mathscr{P}_k \setminus \{k\}} \sqrt{q_j} g_{m,j} \psi^H_k \psi_j + \psi^H_k w^p_m \tag{4}$$

Here, $\psi^H_k w^p_m \sim \mathscr{N}_C(0, \sigma^2 \tau_p)$. By relying on equation (4), we evaluate the quality of CE obtained through various estimators. Besides, we investigate the influence of the perfect knowledge regarding phase-shift using the MMSE estimator called PA-MMSE estimator and no information regarding the phase-shift knowledge using two estimators, namely the MMSE estimator with no phase-shift knowledge called NPA-MMSE estimator and the LS estimator with no knowledge of phase-shift.
In the literature on wireless communication systems, some algorithms are used to estimate the phase-shift, as mentioned in [24,25]. These algorithms require a multi-antenna system and/or a large number of realizations, which is not the purpose of this work.

4.1 Phase-aware MMSE Channel Estimation

4.1.1 Phase-aware MMSE Channel Estimation in coefficient form

This estimator is considered to have perfect knowledge of $\bar{g}_{m,k}$, $\beta_{m,k}$, and $\chi_{m,k}$ at the m_{th} AP where the estimated channel assumed linked the k_{th} user to the m_{th} AP. As mentioned in [26], we can write the estimate channel coefficient based on PA-MMSE as

$$\hat{g}^{pa-mmse}_{m,k} = \bar{g}_{m,k} e^{j\chi_{m,k}} + \frac{\sqrt{q_k}\beta_{m,k}(y^p_{m,k} - \bar{y}^p_{m,k})}{\xi_{m,k}} \tag{5}$$

Here, $\xi_{m,k} = \sum_{l \in \mathscr{P}_k} q_k \tau_p \beta_{m,l} + \sigma^2$ and $\bar{y}_{m,k} = \sum_{l \in \mathscr{P}_k} \sqrt{q_k}\tau_p \bar{g}_{m,k} e^{j\chi_{m,k}}$. It is important to highlight that $\chi_{m,k}$ and $\bar{y}^p_{m,k}$ change in each CB. Hence, $y^p_{m,k}$ also changes in each CB. On the other hand, we assume that $\bar{g}_{m,k}$ and $\beta_{m,k}$ are kept constant for a long-time since they have a relatively slow variation over a long duration. The mean and the variance of estimation error coefficient $\tilde{g}^{pa-mmse}_{m,k} = g^{pa-mmse}_{m,k} - \hat{g}^{pa-mmse}_{m,k}$ are expressed as

$$\begin{cases} \omega_{m,k} = Var\{\tilde{g}^{pa-mmse}_{m,k}\} = \beta_{m,k} - \frac{q_k \tau_p \beta^2_{m,k}}{\xi_{m,k}}, \\ \mathbb{E}\{\tilde{g}^{pa-mmse}_{m,k}\} = \mathbb{E}\{g^{pa-mmse}_{m,k} - \hat{g}^{pa-mmse}_{m,k}\} = 0, \end{cases} \tag{6}$$

The MSE of the PA-MMSE estimator is expressed as

$$\begin{aligned} \Delta_{pa-mmse} &= \mathbb{E}\{|g^{pa-mmse}_{m,k} - \hat{g}^{pa-mmse}_{m,k}|^2\} = \mathbb{E}\{|\tilde{g}^{pa-mmse}_{m,k}|^2\} = Var\{\tilde{g}^{pa-mmse}_{m,k}\}, = \omega_{m,k} \\ &= \beta_{m,k} - \frac{q_k \tau_p \beta^2_{m,k}}{\xi_{m,k}} = \beta_{m,k}(1 - \frac{q_k \tau_p \beta_{m,k}}{\xi_{m,k}}) \end{aligned} \tag{7}$$

The estimated channel coefficient based on PA-MMSE exhibits the following properties

$$\mathbb{E}\{\hat{g}^{pa-mmse}_{m,k} | \chi_{m,k}\} = \bar{g}_{m,k} e^{j\chi_{m,k}}, \tag{8}$$

$$Var\{\hat{g}_{m,k}^{pa-mmse}|\chi_{m,k}\} = \beta_{m,k} - Var\{\tilde{g}_{m,k}^{pa-mmse}\}, \tag{9}$$

It is worth noting that $\hat{g}_{m,k}^{pa-mmse}$ does not follow a Gaussian distribution. In addition, $\tilde{g}_{m,k}^{pa-mmse}$ and $\hat{g}_{m,k}^{pa-mmse}$ are not correlated.
The estimated channel coefficients in this situation are computed locally. In other words, the CE process is not computed in the CPU since each AP is computed the CE itself and does not share it with any other APs as in [5,27,28].

4.1.2 Phase-aware MMSE Channel Estimation in vector form

As an extended version to vector mode, the estimated channel vector expressed as follows

$$\hat{\mathbf{g}}_k^{pa-mmse} = \Upsilon_k \bar{\mathbf{g}}_k + \sqrt{q_k}\mathbf{R}_k \Xi_k^{-1}(\mathbf{y}_k^p - \bar{\mathbf{y}}_k^p) \tag{10}$$

Here, $\bar{\mathbf{g}}_k = [\bar{g}_{1,k}, \ldots, \bar{g}_{M,k}]^T$, $\Upsilon_k = diag(e^{j\chi_{1,k}}, \ldots, e^{j\chi_{M,k}})$, $\mathbf{y}_k^p = [y_{1,k}^p, \ldots, y_{M,k}^p]^T$, $\bar{\mathbf{y}}_k^p = [\bar{y}_{1,k}^p, \ldots, \bar{y}_{M,k}^p]^T$, $\Xi_k = diag(\xi_{1,k}, \ldots, \xi_{M,k})$, and $\mathbf{R}_k = diag(\beta_{1,k}, \ldots, \beta_{M,k})$.
The mean and the covariance of estimation error vector $\tilde{\mathbf{g}}_k^{pa-mmse} = \mathbf{g}_k^{pa-mmse} - \hat{\mathbf{g}}_k^{pa-mmse}$ are expressed as

$$\begin{cases} \Omega_k & = \mathbf{R}_k - q_k \tau_p \mathbf{R}_k \Xi_k^{-1} \mathbf{R}_k \\ \mathbb{E}\{\tilde{\mathbf{g}}_k^{pa-mmse}\} & = 0_M \end{cases} \tag{11}$$

The MSE of PA-MMSE in vector form can be written as

$$\begin{aligned} \Pi^{pa-mmse} &= \mathbb{E}\{|\mathbf{g}_k^{pa-mmse} - \hat{\mathbf{g}}_k^{pa-mmse}|^2\} = \mathbb{E}\{|\tilde{\mathbf{g}}_k^{pa-mmse}|^2\} = Cov\{\tilde{\mathbf{g}}_k^{pa-mmse}\} = Tr(\Omega_k) \\ &= Tr(\mathbf{R}_k - q_k \tau_p \mathbf{R}_k \Xi_k^{-1} \mathbf{R}_k) \end{aligned} \tag{12}$$

The estimated channel vector based on PA-MMSE exhibits the following properties

$$\mathbb{E}\{\hat{\mathbf{g}}_k^{pa-mmse}|\Upsilon_k \bar{\mathbf{g}}_k\} = \Upsilon_k \bar{\mathbf{g}}_k, \tag{13}$$

$$Cov\{\hat{\mathbf{g}}_k^{pa-mmse}|\Upsilon_k \bar{\mathbf{g}}_k\} = \mathbf{R}_k - \Omega_k, \tag{14}$$

4.2 Non-Phase-aware MMSE Channel Estimation

4.2.1 Non-Phase-aware MMSE Channel Estimation in coefficient form

The linear MMSE estimator or the NPA-MMSE estimator is an estimator that has complete knowledge of LSF $\beta_{m,k}$ and $\bar{g}_{m,k}$ coefficients while it has no information regarding phase shift $\chi_{m,k}$. The NPA-MMSE estimate of the channel that links the k_{th} user to the m_{th} AP is expressed as follows:

$$\hat{g}_{m,k}^{npa-mmse} = \frac{\sqrt{q_k}\beta_{m,k}^{'} y_{m,k}^p}{\xi_{m,k}^{'}} \tag{15}$$

Here, $\beta^{'}_{m,k} = \beta_{m,k} + \bar{g}^2_{m,k}$ and $\xi^{'}_{m,k} = \sum_{l \in \mathscr{P}_k} q_k \tau_p (\beta_{m,k} + \bar{g}^2_{m,k}) + \sigma^2 = \sum_{l \in \mathscr{P}_k} q_k \tau_p \beta^{'}_{m,k} + \sigma^2$. The mean and the variance of estimation error coefficient $\tilde{g}^{npa-mmse}_{m,k} = g^{npa-mmse}_{m,k} - \hat{g}^{npa-mmse}_{m,k}$ are expressed as

$$\begin{cases} \omega^{'}_{m,k} = Var\{\tilde{g}^{npa-mmse}_{m,k}\} = \beta^{'}_{m,k} - \frac{q_k \tau_p (\beta^{'}_{m,k})^2}{\xi^{'}_{m,k}} \\ \mathbb{E}\{\tilde{g}^{npa-mmse}_{m,k}\} = 0, \end{cases} \tag{16}$$

The MSE of NPA-MMSE is written as follows

$$\begin{aligned} \Delta^{npa-mmse} &= \mathbb{E}\{|g^{npa-mmse}_{m,k} - \hat{g}^{npa-mmse}_{m,k}|^2\} = \mathbb{E}\{|\tilde{g}^{npa-mmse}_{m,k}|^2\} = Var\{\tilde{g}^{npa-mmse}_{m,k}\}, = \omega^{'}_{m,k} \\ &= \beta^{'}_{m,k} - \frac{q_k \tau_p (\beta^{'}_{m,k})^2}{\xi^{'}_{m,k}} = \beta^{'}_{m,k} (1 - \frac{q_k \tau_p \beta^{'}_{m,k}}{\xi^{'}_{m,k}}) \end{aligned} \tag{17}$$

The estimated channel coefficient based on NPA-MMSE has the following properties

$$\mathbb{E}\{\hat{g}^{npa-mmse}_{m,k}\} = 0, \quad Var\{\hat{g}^{npa-mmse}_{m,k}\} = \beta^{'}_{m,k} - \omega^{'}_{m,k}, \tag{18}$$

4.2.2 Non-Phase-aware MMSE Channel Estimation in vector form

The estimated channel vector based on equation (15) is expressed as follows

$$\hat{\mathbf{g}}^{npa-mmse}_k = \sqrt{q_k} \mathbf{R}^{'}_k (\Xi^{'}_k)^{-1} \mathbf{y}^p_k \tag{19}$$

Here, $\mathbf{y}^p_k = [y^p_{1,k}, \ldots, y^p_{M,k}]^T$, $\Xi^{'}_k = diag(\xi^{'}_{1,k}, \ldots, \xi^{'}_{M,k})$, and $\mathbf{R}^{'}_k = diag(\beta^{'}_{1,k}, \ldots, \beta^{'}_{M,k})$. The mean and the covariance of estimation error vector $\tilde{\mathbf{g}}^{npa-mmse}_k = \mathbf{g}^{npa-mmse}_k - \hat{\mathbf{g}}^{npa-mmse}_k$ are expressed as

$$\begin{cases} \Omega^{'}_k = \mathbf{R}^{'}_k - q_k \tau_p \mathbf{R}^{'}_k (\Xi^{'}_k)^{-1} \mathbf{R}^{'}_k \\ \mathbb{E}\{\tilde{\mathbf{g}}^{npa-mmse}_k\} = \mathbf{0}_M \end{cases} \tag{20}$$

The MSE of NPA-MMSE in vector form is expressed as follows

$$\begin{aligned} \Pi^{npa-mmse} &= \mathbb{E}\{|\mathbf{g}^{npa-mmse}_k - \hat{\mathbf{g}}^{npa-mmse}_k|^2\} = \mathbb{E}\{|\tilde{\mathbf{g}}^{npa-mmse}_k|^2\} = Cov\{\tilde{\mathbf{g}}^{npa-mmse}_k\} = Tr(\Omega^{'}_k) \\ &= Tr(\mathbf{R}^{'}_k - q_k \tau_p \mathbf{R}^{'}_k (\Xi^{'}_k)^{-1} \mathbf{R}^{'}_k) \end{aligned} \tag{21}$$

The estimated channel vector based on NPA-MMSE exhibits the following properties

$$\mathbb{E}\{\hat{\mathbf{g}}^{npa-mmse}_k\} = \mathbf{0}_M, \quad Cov\{\hat{\mathbf{g}}^{npa-mmse}_k\} = \mathbf{R}^{'}_k - \Omega^{'}_k, \tag{22}$$

4.3 LS Channel Estimation

4.3.1 LS Channel Estimation in coefficient form

The traditional LS estimator, which is among the non-bayesian estimators that have no information concerning channel statistic (i.e., LSF $\beta_{m,k}$, $\bar{g}_{m,k}$, and the phase-shift $\chi_{m,k}$) [26], where this estimator aims to minimize the difference between the received signal (i.e., the spread signal) and the desired signal as follows

$$y^p_{m,k} - \sqrt{q_k}\tau_p g_{m,k} = \sum_{j \in \mathscr{P}_k \setminus \{k\}} \sqrt{q_j} g_{m,j} \psi^H_k \psi_j + \psi^H_k w^p_m \tag{23}$$

Where $\mathscr{P}_k$ indicates the group/set of users that uses the same PS as the k_{th} user, including itself. In order to minimizes the aforementioned difference, the equation (23) can be rewritten as follows

$$\left| y^p_{m,k} - \sqrt{q_k}\tau_p g_{m,k} \right|^2 = \left| \sum_{j \in \mathscr{P}_k \setminus \{k\}} \sqrt{q_j} g_{m,j} \psi^H_k \psi_j + \psi^H_k w^p_m \right|^2 \tag{24}$$

The CE expression using this estimator is written as follows

$$\hat{g}^{ls}_{m,k} = \frac{1}{\sqrt{q_k}\tau_p} y^p_{m,k} \tag{25}$$

Where CE using the LS estimator exhibits the following properties

$$\mathbb{E}\{\hat{g}^{ls}_{m,k}\} = 0, \quad Var\{\hat{g}^{ls}_{m,k}\} = \frac{1}{q_k \tau_p} \xi'_{m,k}, \tag{26}$$

The error of estimation is indicated by $\tilde{g}^{ls}_{m,k} = g^{ls}_{m,k} - \hat{g}^{ls}_{m,k}$ which exhibits the following properties

$$\mathbb{E}\{\tilde{g}^{ls}_{m,k}\} = 0, \quad Var\{\tilde{g}^{ls}_{m,k}\} = \frac{1}{q_k \tau_p} \xi'_{m,k} - \beta'_{m,k}, \tag{27}$$

4.3.2 LS Channel Estimation in vector form

The CE expression using LS estimator (in vector form) is written as follows

$$\hat{\mathbf{g}}^{ls}_k = \frac{1}{\sqrt{q_k}\tau_p} \mathbf{y}^p_k \tag{28}$$

Here, $\mathbf{y}^p_k = [y^p_{1,k}, \ldots, y^p_{M,k}]^T$ is a vector form, thereby the CE using the LS estimator exhibits the following properties

$$\mathbb{E}\{\hat{\mathbf{g}}^{ls}_k\} = \mathbf{0}_M, \quad Cov\{\hat{\mathbf{g}}^{ls}_k\} = \frac{1}{q_k \tau_p} \Xi'_k, \tag{29}$$

The error of estimation is indicated by $\tilde{\mathbf{g}}^{ls}_k = \mathbf{g}^{ls}_k - \hat{\mathbf{g}}^{ls}_k$ which has the following properties

$$\mathbb{E}\{\tilde{\mathbf{g}}^{ls}_k\} = \mathbf{0}_M, \quad Cov\{\tilde{\mathbf{g}}^{ls}_k\} = \frac{1}{q_k \tau_p} \Xi'_k - R'_k, \tag{30}$$

After having given the MSE expressions for each estimator in both forms. This table below summarize the MSE expressions that are obtained for all estimator for coefficient and vector forms

The MSE expressions for all estimator		
Estimator	MSE expression in the case of channel coefficient	MSE expression in the case of channel vector
PA-MMSE Estimator	$\Delta^{pa-mmse} = \beta_{m,k}(1 - \frac{q_k\tau_p\beta_{m,k}}{\xi_{m,k}})$	$\Pi^{pa-mmse} = Tr(\mathbf{R}_k - q_k\tau_p\mathbf{R}_k\Xi_k^{-1}\mathbf{R}_k)$
NPA-MMSE Estimator	$\Delta^{npa-mmse} = \beta'_{m,k}(1 - \frac{q_k\tau_p\beta'_{m,k}}{\xi'_{m,k}})$	$\Pi^{npa-mmse} == Tr(\mathbf{R}'_k - q_k\tau_p\mathbf{R}'_k(\Xi'_k)^{-1}\mathbf{R}'_k)$
LS Estimator	$\Delta^{ls} = \frac{1}{q_k\tau_p}\xi'_{m,k} - \beta'_{m,k}$	$\Pi^{ls} = \frac{1}{q_k\tau_p}\Xi'_k - R'_k,$

Table 1 The MSE expressions that are obtained for all estimator for coefficient and vector forms

5 Numerical Result and Discussions

The purpose of this section is to affirm our numerical expression provided in the previous sections. We treat the CF M-MIMO in which $M = 100$ APs (except for Figure (4), where the number of APs is varied) and $K = 40$ users are deployed where the distribution of either APs and users is a uniform distribution within the area. Besides, this area is considered to be a square of dimension $1000 \times 1000\ m^2$ (except for Figure (2), where the area dimension is varied). Furthermore, we consider that the CB length is setting to $\tau_c = 200$ samples, the PS length is setting to $\tau_p = 5$ ($\tau_p << K$, as indicates in the previous section), and UL power is setting to $q = 200$ mW. On the other hand, the pilot assignment/allocation to each user is assigned in such a manner that this user receives lower interference. In other words, the first τ_p pilots are assigned randomly to the first τ_p users, whereas the remaining users assign with pilots in order to give the lowest interference levels to the users in the actual set of pilots (i.e., $\mathscr{P}_k$).

We implement LSF using the *COST* 321 *Walfish-Ikegami* model for the micro-cells scenario, as shown in [29]. Furthermore, we address the situation in which APs are consider positioned at the height of 12.5 m while users are consider positioned at the height of 1.5 m. We consider that only the LoS path that links each user to its serving AP. One can ask the question of why we have considered the LoS path between each

user-AP pairs. We have investigated the LoS path in order to represent the mean of the channel gain that is given in equation (1). Therefore, the adopted path-loss model is expressed as follows

$$\theta_{m,k} = -30.18 - 10\eta log_{10}(\frac{d_{m,k}}{1m}) + \Gamma_{m,k} \tag{31}$$

Here, $d_{m,k}$ indicates the distance between the m_{th} AP and the k_{th} user and η indicates the path-loss exponent (η is setting to 2.6 for all numerical results except for Figure (5), in which η is varied). The coefficient $\Gamma_{m,k}$ indicates the shadowing. The Rician parameter is in function of the distance $d_{m,k}$ as follows

$$\kappa_{m,k} = 10^{1.3-0.003d_{m,k}} \tag{32}$$

This work studied correlated-shadowing as reported in [5], where $\Gamma_{m,k}$ is expressed as follows

$$\Gamma_{m,k} = \sqrt{\delta}\mu_m + \sqrt{1-\delta}\nu_k, \tag{33}$$

Here, $\mu_m \sim \mathcal{N}(0, \sigma_{sf}^2)$, and $\nu_k \sim \mathcal{N}(0, \sigma_{sf}^2)$ symbolize the effect of blockage provided by the large obstacles in the neighborhood of the m_{th} AP and the k_{th} user, respectively. The parameter δ symbolizes the shadowing, which obeys the following inequality $0 \leq \delta \leq 1$. The covariance of users pair or APs pair is computed based on the following equations (i.e., equations (34), (35))

$$\mathbb{E}\{\mu_m \mu_n\} = 2^{-\frac{d_{m,n}}{d_{dc}}} \tag{34}$$

Here, $d_{m,n}$ indicates the distance between the m_{th} AP and n_{th} AP, where d_{dc} indicates the decorrelation distance, which relies on the propagation environment.

$$\mathbb{E}\{\nu_k \nu_j\} = 2^{-\frac{d_{k,j}}{d_{dc}}} \tag{35}$$

Here, $d_{k,j}$ indicates the distance between the k_{th} user and j_{th} user. For the decorrelation distance, we assume the same value for both situations (i.e., $d_{dc} = 100$ same decorrelation distance). We setting the factors $\sigma_{sf} = 8$ and $\delta = 0.5$. Besides, The LSF, as well as $\bar{g}_{m,k}$ are computed based on the Rician factor and the path loss model as

$$\bar{g}_{m,k} = \sqrt{\frac{\kappa_{m,k}}{\kappa_{m,k}+1}}\sqrt{\theta_{m,k}}, \quad \beta_{m,k} = \frac{1}{\kappa_{m,k}+1}\theta_{m,k} \tag{36}$$

Before evaluating our simulation result, we bring to your attention that analytical and simulated results are introduced for the PA-MMSE and NPA-MMSE estimators, while analytical results are given for the LS estimator.

In figure (2), the MSE is plotted against the area size, where the parameters' value are previously defined (i.e.,M, K, q,....). This figure is introduced to evaluate the performance of the estimators used regarding the area dimension used. The performance of PA-MMSE, NPA-MMSE, and the LS estimators are compared with respect to the area size. As expected, better performance is achieved through the PA-MMSE estimator since the PA-MMSE estimator has complete knowledge of the phase-shift, the LSF coefficient, and the channel average $\bar{\mathbf{g}}_k$, while the performance obtained with the

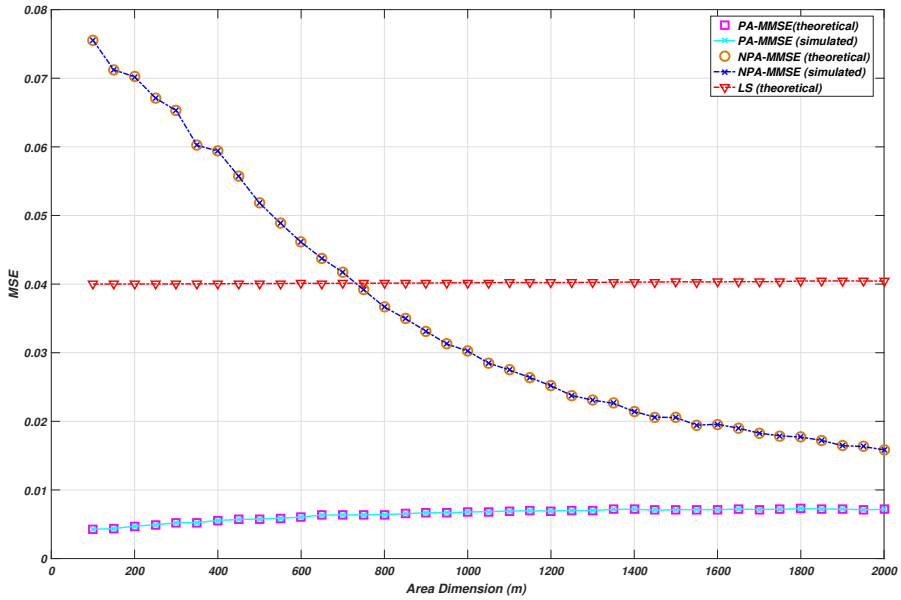


Fig. 2 The MSE in respect to the area dimension

NPA-MMSE estimator is relying on the area dimension used. When the area dimensions range is between [100 m, 700 m], the NPA-MMSE estimator provides the worst performance compared to the LS estimator. Furthermore, when the area dimension range superior to 700 m, the NPA-MMSE estimator offers better performance compared to the LS estimator. As the area dimension increases the performance provided using the NPA-MMSE estimator approaches the PA-MMSE estimator's performance. The asymptotic behavior provided by the NPA-MMSE estimator is explained due to the fact that, as the area dimension increase, the phase-shift influence reduce. In other words, when the area dimension increase, a large gap between each pair of users and each pair of APs is more expect to be created. Hence, the effect of phase-shift knowledge is not important.

In figure (3), the MSE is plotted against the number of users, K. This Figure is introduced to evaluates the estimators' performance when a different number of users are served in the network. The performance of PA-MMSE, PA-MMSE, and the LS estimators are compared with respect to the number of users in the network. As expected, the best performance is obtained by the PA-MMSE estimator since the PA-MMSE estimator has complete knowledge of the phase shift, the LSF coefficient and the channel mean $\bar{\mathbf{g}}_k$, while the performance obtained by the LS estimator is the worst. When the number of users in the network is equal to 5 (no pilots are reused, all used pilots are orthogonal to each other because $\tau_p = 5$), we notice that the PA-MMSE and NPA-MMSE perform similarly, whereas the LS provided the worst performance even if a small number of users in the network (constant MSE values for all the users range). As the number of serving user increase, the NPA-MMSE estimator provides increased MSE values compared to PA-MMSE. This can be explained by the fact

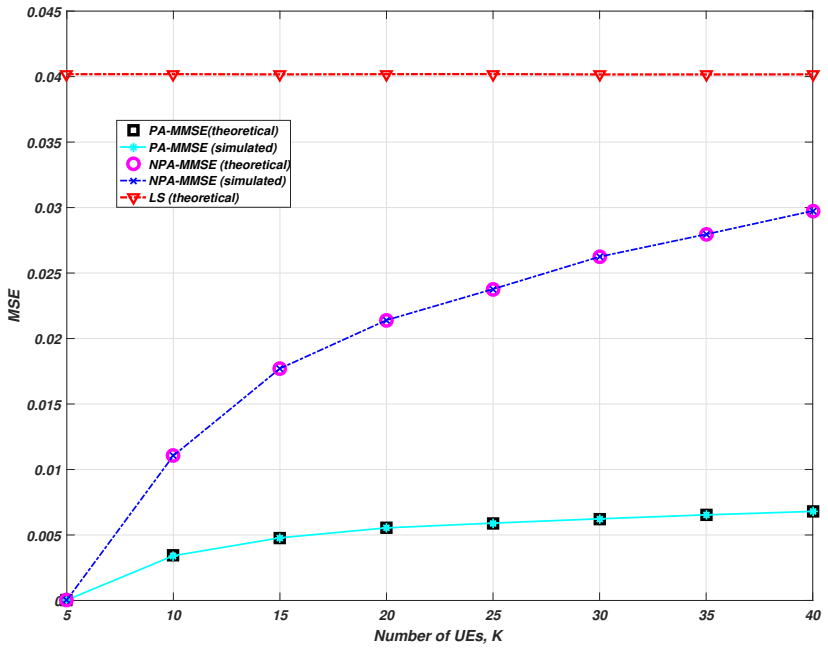


Fig. 3 The MSE in respect to the number of users, K

that when the number of users increases a small gap between each pair of users is more expected to be created (since the users are randomly distributed). Hence, the effect of phase-shift knowledge is more important in order to achieve better channel estimation.

In figure (4), the MSE is plotted against the number of APs in the network, M. The performance of PA-MMSE, the PA-MMSE, and the LS estimators are compared with respect to the number of APs in the network. We emphasize that during this work, we assume single antenna APs. As indicates from the figure, better performance is achieved by the PA-MMSE estimator since the PA-MMSE estimator has complete knowledge of the phase-shift, the LSF coefficient, and the channel average $\bar{\mathbf{g}}_k$. Besides, The worst performance is provided by the traditional LS estimator. The performance obtained by the NPA-MMSE estimator is much better than the LS estimator. The obtained gap between the PA-MMSE estimator and the PA-MMSE estimator in terms of the MSE metric can be explained by the fact that the knowledge of the phase shift. In conclusion, phase shift knowledge is an important factor for the CE process.

In figure (5), the MSE is plotted against various path-loss exponent values, η. The performance provided by PA-MMSE, the PA-MMSE, and the LS estimators is compared with respect to various path-loss exponent values. As indicates from the figure, better performance is achieved by the PA-MMSE estimator where it provides the

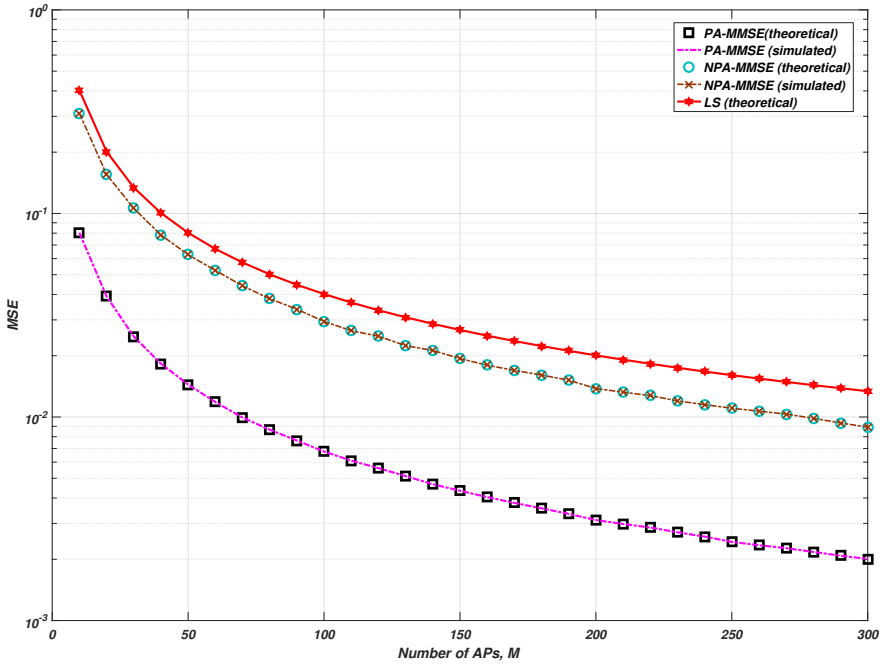


Fig. 4 The MSE with respect to the number of APs, M

low MSE values. Resulting from the fact that the PA-MMSE estimator has complete knowledge of the phase-shift, the LSF coefficient, and the channel average $\bar{\mathbf{g}}_k$. Furthermore, The worst performance is provided by the traditional LS estimator, where for $\eta \geq 3.5$, higher performance degradation is obtained. The performance obtained by the NPA-MMSE estimator is much better than the LS estimator, where the NPA-MMSE estimator provides results comparable to the PA-MMSE estimator (regarding LS estimator, since LS provides a higher degradation result, which is obvious for high η values) even if when a large value of the path-loss exponent. Notice that, in the standard situation in which η is setting to 2.6, the LS and NPA-MMSE estimators perform similarly a little taken, whereas the NPA-MMSE estimator provided better performance due to the phase-shift knowledge.

6 Conclusion

This work has studied the CE for CF M-MIMO in the UL phase and considered the Rician fading channel where the LOS path is realized with a phase-shift that models the users' mobility wherein the considered phase-shift follows a uniform distribution. The performances of different estimators have evaluated, discussed, and compared in various situations. We have assumed the scenario in which each AP has prior knowledge of channel statistics. We have concluded that phase-shift knowledge is an important task for the CE process since the PA-MMSE estimator presents a better per-

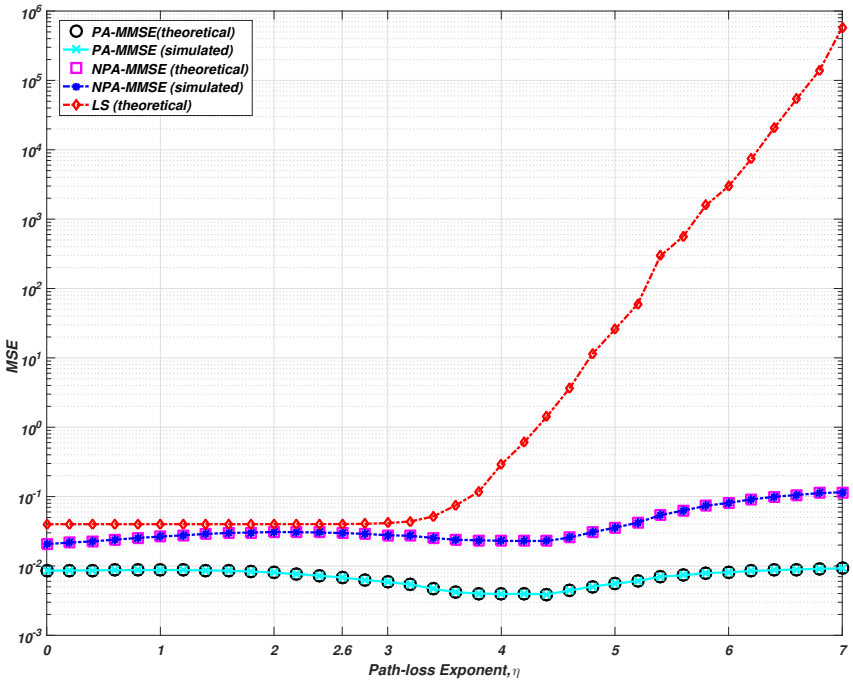


Fig. 5 The MSE with respect to the path-loss exponent, η

formance in all studied situations (The performances have evaluated using the MSE metric), whereas the PA-MMSE estimator provides results relatively lower than the PA-MMSE estimator. Furthermore, we have affirmed that when the area dimension increases, the phase-shift influence is reduced (as the area dimension increase, the NPA-MMSE estimator has provided asymptotically result to the PA-MMSE estimator). As the area dimension increases, a large gap between each user pair and each AP pair is more likely to occur. Hence, the impact of phase-shift knowledge diminishes. On the other hand, analytical and simulated results have provided for the PA-MMSE estimator and the NPA-MMSE estimator, which have yielded similar results.

References

1. Thomas L Marzetta and Hien Quoc Ngo. *Fundamentals of massive MIMO*. Cambridge University Press, 2016.
2. Thomas L Marzetta. Noncooperative cellular wireless with unlimited numbers of base station antennas. *IEEE transactions on wireless communications*, 9(11):3590–3600, 2010.
3. Hong Yang and Thomas L Marzetta. A macro cellular wireless network with uniformly high user throughputs. In *2014 IEEE 80th Vehicular Technology Conference (VTC2014-Fall)*, pages 1–5. IEEE, 2014.
4. Mona Jaber, Muhammad Ali Imran, Rahim Tafazolli, and Anvar Tukmanov. 5g backhaul challenges and emerging research directions: A survey. *IEEE access*, 4:1743–1766, 2016.

5. Hien Quoc Ngo, Alexei Ashikhmin, Hong Yang, Erik G Larsson, and Thomas L Marzetta. Cell-free massive mimo versus small cells. *IEEE Transactions on Wireless Communications*, 16(3):1834–1850, 2017.
6. Kien T Truong and Robert W Heath. The viability of distributed antennas for massive mimo systems. In *2013 Asilomar Conference on Signals, Systems and Computers*, pages 1318–1323. IEEE, 2013.
7. Giovanni Interdonato, Emil Björnson, Hien Quoc Ngo, Pål Frenger, and Erik G Larsson. Ubiquitous cell-free massive mimo communications. *EURASIP Journal on Wireless Communications and Networking*, 2019(1):1–13, 2019.
8. Emil Björnson, Randa Zakhour, David Gesbert, and Björn Ottersten. Cooperative multicell precoding: Rate region characterization and distributed strategies with instantaneous and statistical csi. *IEEE Transactions on Signal Processing*, 58(8):4298–4310, 2010.
9. Hien Quoc Ngo, Alexei Ashikhmin, Hong Yang, Erik G Larsson, and Thomas L Marzetta. Cell-free massive mimo: Uniformly great service for everyone. In *2015 IEEE 16th international workshop on signal processing advances in wireless communications (SPAWC)*, pages 201–205. IEEE, 2015.
10. Shidong Zhou, Ming Zhao, Xibin Xu, Jing Wang, and Yan Yao. Distributed wireless communication system: a new architecture for future public wireless access. *IEEE Communications Magazine*, 41(3):108–113, 2003.
11. Kien T Truong and Robert W Heath. The viability of distributed antennas for massive mimo systems. In *2013 Asilomar Conference on Signals, Systems and Computers*, pages 1318–1323. IEEE, 2013.
12. Wan Choi and Jeffrey G Andrews. Downlink performance and capacity of distributed antenna systems in a multicell environment. *IEEE transactions on wireless communications*, 6(1):69–73, 2007.
13. Daniel Castanheira and Atilio Gameiro. Distributed antenna system capacity scaling [coordinated and distributed mimo]. *IEEE Wireless Communications*, 17(3):68–75, 2010.
14. Robert Heath, Steven Peters, Yi Wang, and Jiayin Zhang. A current perspective on distributed antenna systems for the downlink of cellular systems. *IEEE Communications Magazine*, 51(4):161–167, 2013.
15. Emil Bjornson, Niklas Jalden, Mats Bengtsson, and Björn Ottersten. Optimality properties, distributed strategies, and measurement-based evaluation of coordinated multicell ofdma transmission. *IEEE Transactions on Signal Processing*, 59(12):6086–6101, 2011.
16. Özgecan Özdogan, Emil Björnson, and Jiayi Zhang. Performance of cell-free massive mimo with rician fading and phase shifts. *IEEE Transactions on Wireless Communications*, 18(11):5299–5315, 2019.
17. Giovanni Interdonato, Hien Quoc Ngo, Erik G Larsson, and Pål Frenger. On the performance of cell-free massive mimo with short-term power constraints. In *2016 IEEE 21st International Workshop on Computer Aided Modelling and Design of Communication Links and Networks (CAMAD)*, pages 225–230. IEEE, 2016.
18. Emil Björnson and Luca Sanguinetti. Scalable cell-free massive mimo systems. *IEEE Transactions on Communications*, 68(7):4247–4261, 2020.
19. Jiayi Zhang, Yinghua Wei, Emil Björnson, Yu Han, and Shi Jin. Performance analysis and power control of cell-free massive mimo systems with hardware impairments. *IEEE Access*, 6:55302–55314, 2018.
20. Zhe Wang, Jiayi Zhang, Emil Björnson, and Bo Ai. Uplink performance of cell-free massive mimo over spatially correlated rician fading channels. *IEEE Communications Letters*, 2020.
21. Trang C Mai, Hien Quoc Ngo, and Trung Q Duong. Cell-free massive mimo systems with multi-antenna users. In *2018 IEEE Global Conference on Signal and Information Processing (GlobalSIP)*, pages 828–832. IEEE, 2018.
22. Emil Björnson, Jakob Hoydis, and Luca Sanguinetti. Massive mimo networks: Spectral, energy, and hardware efficiency. *Foundations and Trends in Signal Processing*, 11(3-4):154–655, 2017.
23. Thomas L Marzetta and Hien Quoc Ngo. *Fundamentals of massive MIMO*. Cambridge University Press, 2016.
24. Arogyaswami Paulraj, Richard Roy, and Thomas Kailath. Estimation of signal parameters via rotational invariance techniques-esprit. In *Nineteeth Asilomar Conference on Circuits, Systems and Computers, 1985.*, pages 83–89. IEEE, 1985.
25. Ralph Otto Schmidt. A signal subspace approach to multiple emitter location and spectral estimation. 1982.
26. Steven M Kay. *Fundamentals of statistical signal processing*. Prentice Hall PTR, 1993.
27. Elina Nayebi, Alexei Ashikhmin, Thomas L Marzetta, Hong Yang, and Bhaskar D Rao. Precoding and power optimization in cell-free massive mimo systems. *IEEE Transactions on Wireless Communications*, 16(7):4445–4459, 2017.

28. Elina Nayebi, Alexei Ashikhmin, Thomas L Marzetta, and Hong Yang. Cell-free massive mimo systems. In *2015 49th Asilomar Conference on Signals, Systems and Computers*, pages 695–699. IEEE, 2015.
29. 3rd generation partnership project, technical specification group radio access network; spatial channel model for multiple input multiple output (mimo) simulations. 3GPP TR 25.996 V14.0.0, Mar. 2017.

Figures

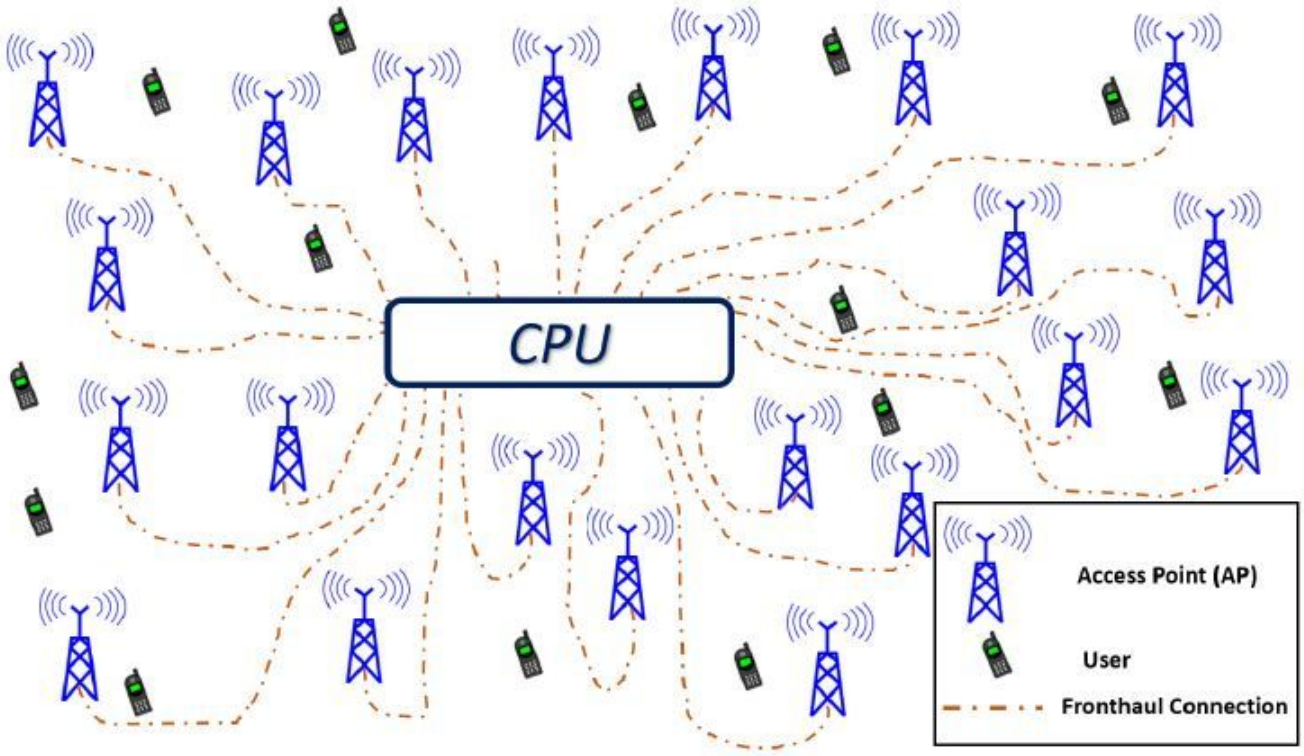


Figure 1

Typical representation of a CF M-MIMO grid

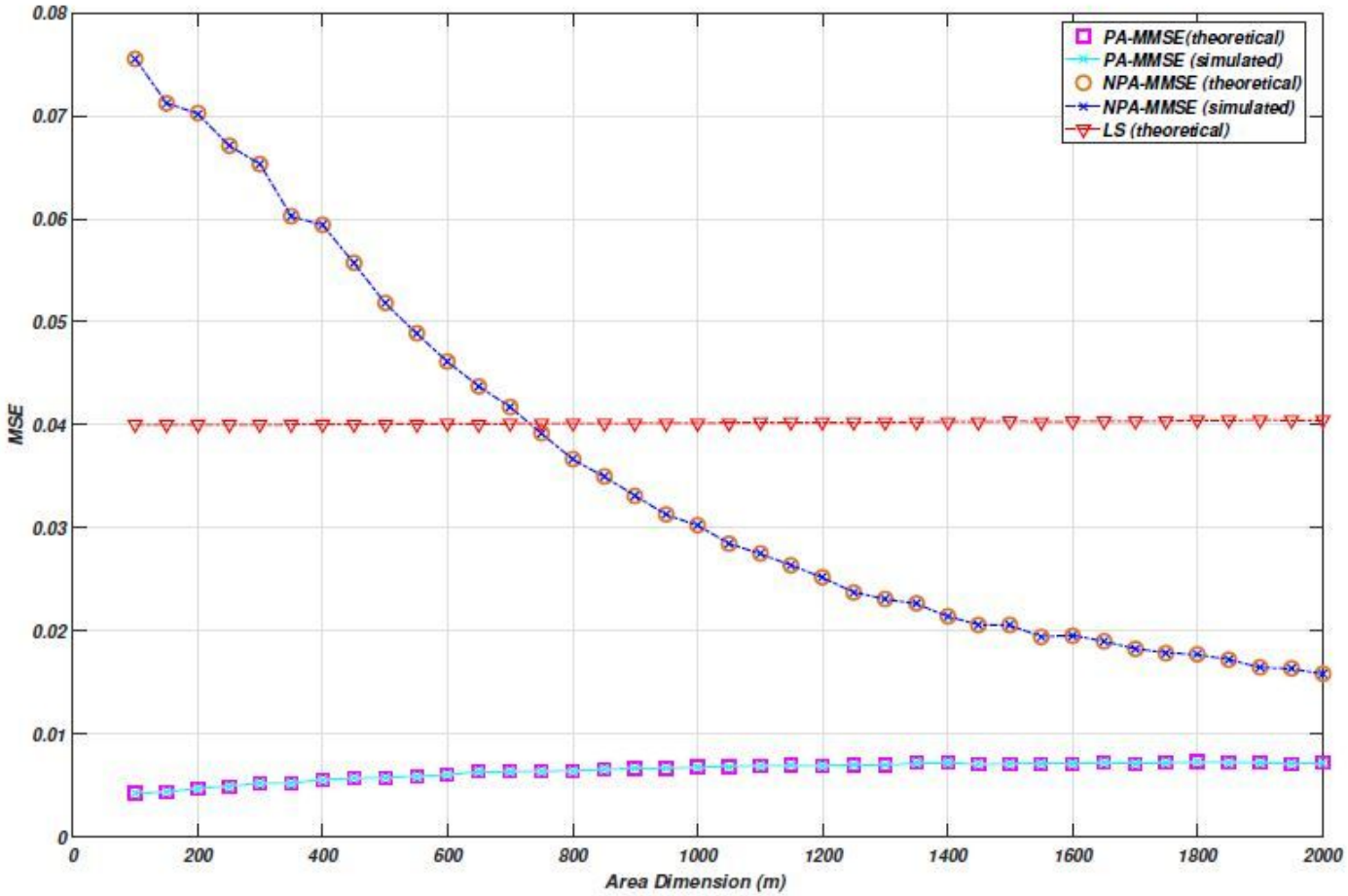


Figure 2

The MSE in respect to the area dimension

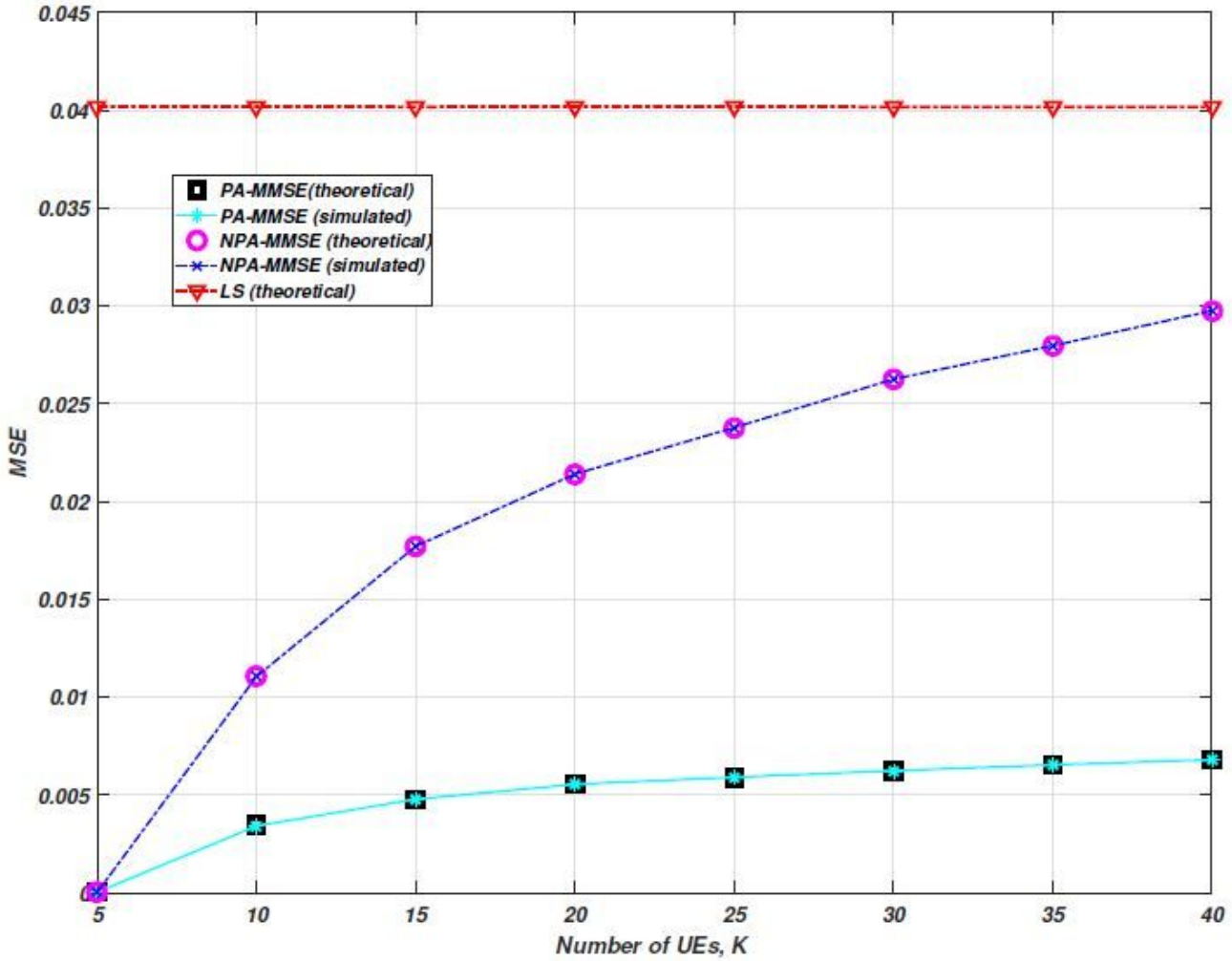


Figure 3

The MSE in respect to the number of users, K

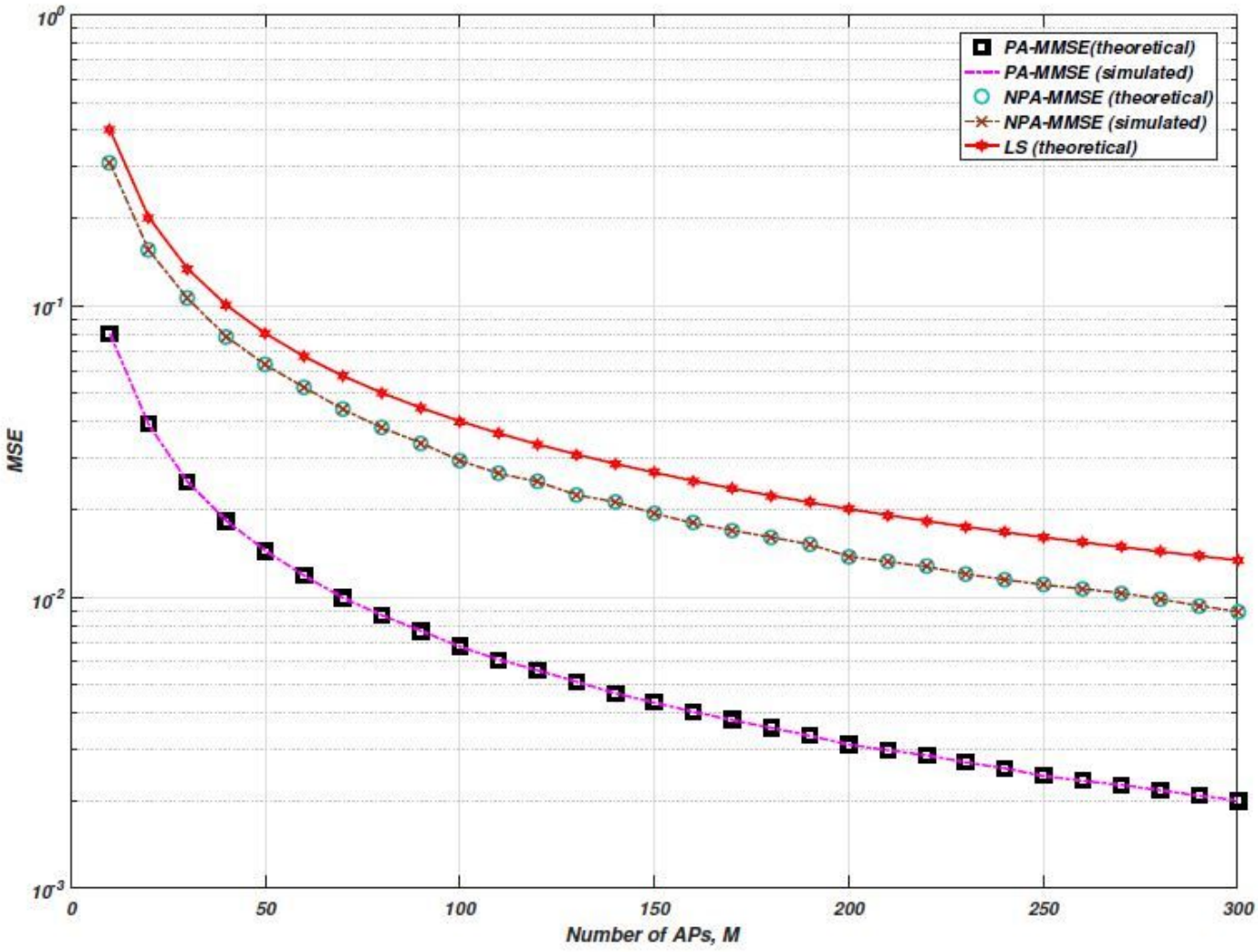


Figure 4

The MSE with respect to the number of APs, M

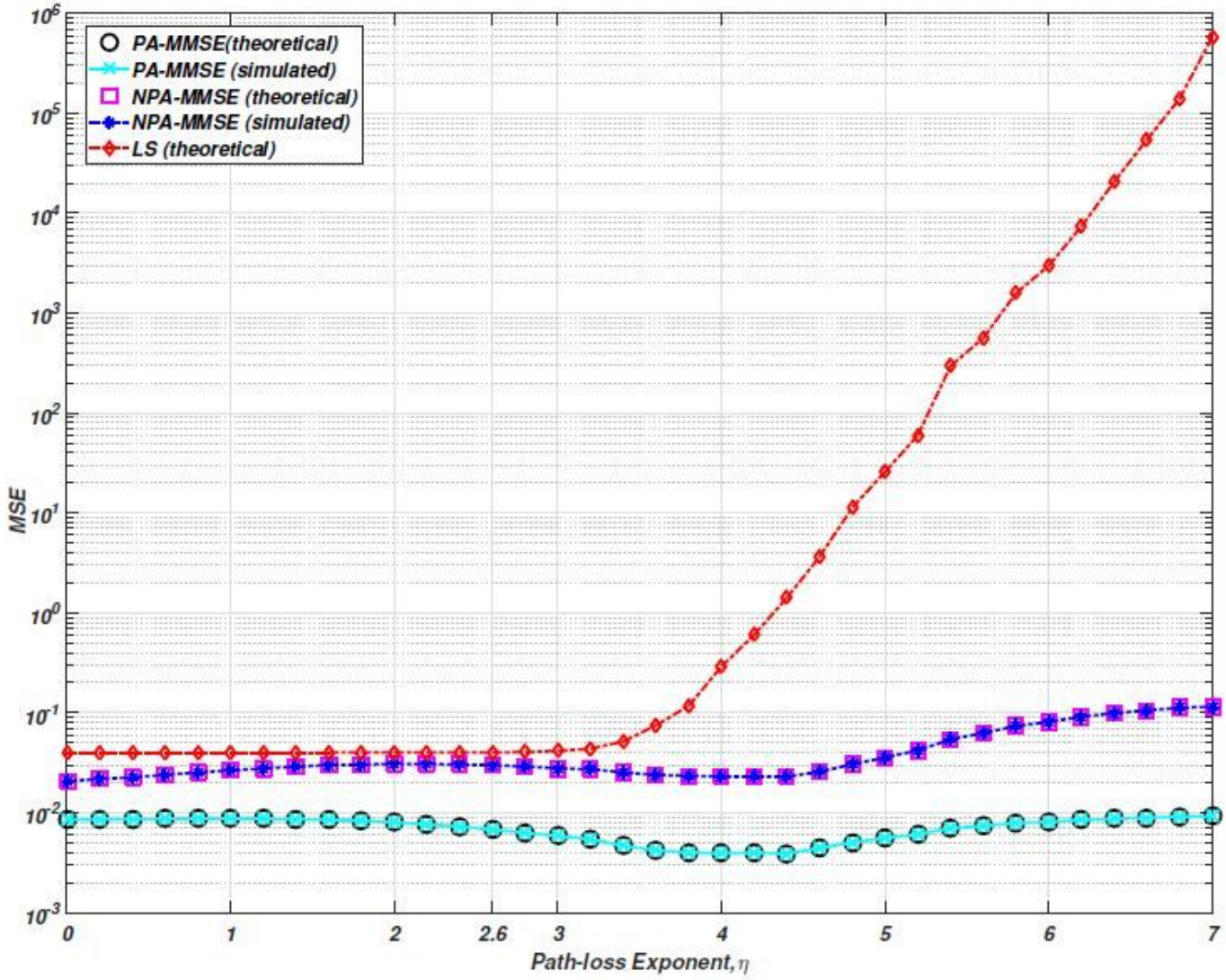


Figure 5

The MSE with respect to the path-loss exponent, h